Experimental validation of the coupled fluid flow, heat transfer and electromagnetic numerical model of the medium-power dry-type electrical transformer

Jacek Smolka *, Andrzej J. Nowak

Institute of Thermal Technology, Silesian University of Technology, Konarskiego 22, 44-100 Gliwice, Poland

Abstract

This paper presents experimental validation of a numerical model of coupled processes within a three-phase medium-power dry-type electrical transformer. The analysis carried out employed a multi-disciplinary approach involving heat, fluid flow and electromagnetics. The thermal and fluid flow analysis was coupled with an electromagnetic model in order to examine the specific power losses within the coils and the core. The thermal boundary conditions, i.e. the local and temperature-dependent heat fluxes, were computed by considering a numerical model of the surrounding internal and external air. Moreover, separate numerical and analytical models were considered in order to obtain the anisotropic thermal conductivities for different types of coils and also for laminated cores. To validate the numerical model, experimental transformer temperature tests in the short-circuit, open-circuit, and under nominal parameters according to the current European Standards for dry-type transformers were performed. During the tests, temperatures were measured at selected points on elements of the transformer using thermocouples and thermometers, while on the external tank walls an infrared thermography was employed. The obtained numerical results showed that the prediction of the temperature distribution within the analyzed transformers and their surroundings was very accurate.
© 2007 Elsevier Masson SAS. All rights reserved.

Keywords: Dry-type transformer; Numerical model; Validation; Local heat generation; Coupled problem

1. Introduction

In the design process of electrical transformers, one of the most important issues is an accurate prediction of the location of the hot spot occurring in the device, especially in the core and coils. The temperature level in these elements directly influences the power losses and durability of the transformers. This means that the analysis of the physical processes in such units is of a multidisciplinary nature and should be considered as strongly coupled phenomena [1,2]. In order to consider these challenging problems, a numerical analysis involving thermal, fluid flow and electromagnetic coupling should be applied.

In the transformer literature, many research papers are devoted to particular aspects of the transformer operation, cooling, design, etc. For instance, in [3] calculations of the eddy current losses in a laminated core are presented on the basis of a single laminate of the transformer core. The authors of [4,5] considered a detailed analysis of the cooling processes in the windings of a disc-type transformer. However, a drawback of these approaches is that they are uncoupled. Apart from these investigations, in the subject literature, the authors have considered coupled problems and most of them are thermal-electromagnetic couplings [1,2]. However, the couplings are very often very simplified and rather average quantities instead of local ones are taken into account. In such analyses, a typical definition of the convective and/or radiative boundary conditions utilizes the average wall temperatures and the average Nusselt numbers on particular boundaries [6,7]. Similarly, typical procedures for the determination of transformer losses assume that the heat is generated uniformly within the whole volume of the device coils and core [8–10]. More-

---

* Corresponding author. Tel.: +48 32 237 10 19; fax: +48 32 237 28 72.
  E-mail address: jacek.smolka@polsl.pl (J. Smolka).

Nomenclature

Latin symbols

$\boldsymbol{A}$	magnetic vector potential	T m
A	area	m^2
a	absorption coefficient	m^{-1}
$\boldsymbol{B}$	magnetic flux vector	T
$C_{1\varepsilon}, C_{2\varepsilon}, C_{3\varepsilon}$	empirical constants in the transport equation for the turbulent dissipation rate	
c	specific heat	$J\,kg^{-1}\,K^{-1}$
$\boldsymbol{E}_c$	electric field vector	$V\,m^{-1}$
$\boldsymbol{F}$	body force vector	$N\,m^{-3}$
f	frequency	Hz
G_b	generation of turbulence kinetic energy due to buoyancy	$kg\,m^{-1}\,s^{-3}$
G_k	generation of turbulence kinetic energy due to mean velocity gradients	$kg\,m^{-1}\,s^{-3}$
I_c	current	A
I	radiation intensity	$W\,m^{-2}\,sr$
$\boldsymbol{J}_c$	current density vector	$A\,m^{-2}$
K	turbulent kinetic energy	$m^2\,s^{-2}$
k	thermal conductivity	$W\,m^{-1}\,K^{-1}$
L	length	m
m_{St}	coefficient in Steinmetz equation	
M	molar mass	$kg\,kmol^{-1}$
n_{St}	exponent in Steinmetz equation	
n	refractive index	
P	electric power	V A
p	pressure	Pa
Q_r	total radiative heat transfer rate	W
q_v	volumetric heat source	$W\,m^3$
R_c	winding resistance	Ω
R_c	gas constant	$J\,kg^{-1}\,K^{-1}$
$\boldsymbol{r}$	position vector	
$\boldsymbol{s}$	scattering direction vector	

$\boldsymbol{s}_s$	direction vector	
t	temperature	°C
U	voltage	V
V_c	electric scalar potential	V
$\boldsymbol{w}$	velocity vector	$m\,s^{-1}$
$\boldsymbol{w}_c$	velocity of charge particles	$m\,s^{-1}$
$x,\ y,\ z$	Cartesian coordinates	m

Greek symbols

ΔP_{Cu}	total coil power loss	W
ΔP_{Fe}	total core power loss	W
Δt	total winding temperature rise	°C
Δt_c	winding temp. rise in short-circuit test	°C
Δt_e	winding temp. rise in open-circuit test	°C
ε	turbulent dissipation rate	$m^2\,s^{-3}$
μ	dynamic viscosity	$N\,s\,m^{-2}$
μ_c	magnetic permeability	$T\,m\,A^{-1}$
μ_t	turbulent viscosity	$kg\,m^{-2}\,s^{-2}$
Ω	solid angle	sr
Φ	phase function	
ρ	density	$kg\,m^{-3}$
σ	Stefan–Boltzmann constant	$W\,m^{-2}\,K^{-4}$
σ_K	turbulent Prandtl number for turbulent kinetic energy	
σ_s	scattering coefficient	m^{-1}

Subscripts

op	operating
w	wall
∞	ambient
S	boundary
max	maximum
eff	effective
i	ith direction

over, in the formulation of the mathematical model for the transformer, attention should be paid to its proper and accurate modelling in terms of the thermal properties. In [11] the theoretical determination of anisotropic effective thermal conductivities for typical winding configurations was described, while in [12] a numerical model for the effective thermal conductivities superconducting coil is presented. However, these works were not applied to any more complex transformer systems.

Since the coupled processes in most electrical transformer analyzes are not considered, or the existing coupling procedures are very simplified, the general aim of this paper was to create, solve and validate a numerical model of the coupled thermal-flow-electromagnetic phenomena that occurs within such a device. The present paper is a continuation of the work on numerical modelling of the coupled processes occurring in electrical dry-type transformers. The developed mathematical model has been already applied to a low power cast resin unit working in

a laboratory environment [13]. Currently, a real medium-power transformer was numerically analyzed and experimentally validated. To accomplish this general task, numerous partial problems were analyzed and the following quantities were determined:

– Local and temperature-dependent transformer electromagnetic energy losses in both the core and windings. Calculations of the coil losses, known as the Joule heat, were performed on the basis of the local current flux assuming that the electrical resistivity is a temperature-dependent quantity. In the case of the core loss, the Steinmetz-based equation approach was employed.

– Local and temperature-dependent distribution of both convective and radiative heat fluxes as boundary conditions. This was achieved taking into account the air flow inside and outside the tank of the device. It is also worth mentioning that the idea of local heat fluxes can be successfully

applied to any transformer working in an arbitrary surrounding.

– Both electromagnetic and thermal material temperature-dependent properties have been applied in the coupled analyses.

– Anisotropic thermal material properties for the core, and especially for the windings. The core consists of laminates and its thermal conductivity across laminates is not the same as along them. In coils, the thermal conductivity is much larger along wires than in the cross-sectional plane of the wires. Therefore, for the core in each direction and for the coils along the wires, analytical models were used to determine the effective values of these properties. However, for both directions in the cross-sectional plane to the wires, these values were obtained numerically.

The considered unit and the low power cast resin devices (analyzed also in one of the previous works [13]) have been selected since they are good representatives among other dry-type transformers. Due to the different internal construction, the device position in the tank and finally cooling system, a simulation model is able to answer the question of the most effective heat transfer mode for the heat removal for this group of devices. Additionally, the procedures of the coupled thermal, fluid flow and electromagnetic processes in dry-type transformers developed within this paper can easily be extended to the most common oil-cooled devices. It only requires a redefinition of the material properties for different types of the coolant.

Mathematical models and procedures presented within the paper may be applied during both the design process and transformer operation. In particular, this analysis can be useful in situations where the device works in rigorous conditions in terms of heat removal. In the paper, a three phase medium power dry-type naturally cooled electrical transformer was considered. The device is a part of the prototype transformer station designed to supply the electric equipment and machines in the underground mining headings, which are classified as dangerous due to possible methane and/or coal dust explosions. Therefore, the developed numerical model embraced not only the unit itself but also its environment, i.e. transformer tank, internal and external air. Also such an approach allowed the authors to perform a more detailed experimental validation of the transformer station.

Validation of the computational results obtained from the developed mathematical model was carried out utilizing experimental data. The experimental transformer temperature tests consisted of runs in the short-circuit and open-circuit according to the current European Standards for dry-type transformers [14]. During these experimental tests, temperatures were measured at selected points on the transformer elements (e.g. coils, core) using thermocouples and/or on external tank walls using an infrared camera. In addition, information on the temperature field was captured from the internal and external air surrounding the device and the tank.

2. General procedures for the numerical model definition of the dry-type transformer

The coupling procedure was started from the Fluent computations [15]. The mathematical model required the solution of the thermal-flow problem including the governing equations, source terms, boundary conditions and material properties. It should be stressed that the thermal conductivities were defined as anisotropic and effective values in each direction for the core and the coils. The numerical analyses aiming at the determination of the conductivities for the coils were performed as separate test cases. Then the calculated quantities were introduced into the thermal and fluid flow model. In the first run of these processes for the whole transformer and its surroundings, the solution was obtained using the average and uniform heat sources in the governing equations. In this case, the power losses in the transformer core and coils, based on experimental measurements in the open-circuit and short-circuit tests, were determined. The obtained temperature field was transferred to the electromagnetic solver to define the local and temperature-dependent electric resistivity for the windings.

In the electromagnetic solver Ansys/Emag [16], the governing equations and the boundary conditions were specified. Then the material properties for the coils were completed on the basis of the temperature distribution from the CFD model. As a result of this run, the local fields of the transformer losses from the coils and core were obtained. The values determined for each individual mesh cell for these transformer elements were used to define the heat sources in the governing energy equation of the thermal and fluid flow analysis.

In the consecutive iterations, the CFD solver generated a new temperature field to update the value of the electrical resistivity, and the electromagnetic code using this information recalculated the transformer heat losses. The procedure was continued until the variations of the updated quantities became negligible. The coupling of the thermal, fluid flow and electromagnetic solutions is schematically depicted in Fig. 1. Details of each step of the numerical model formulation as shown in this figure are presented in the following two sections.
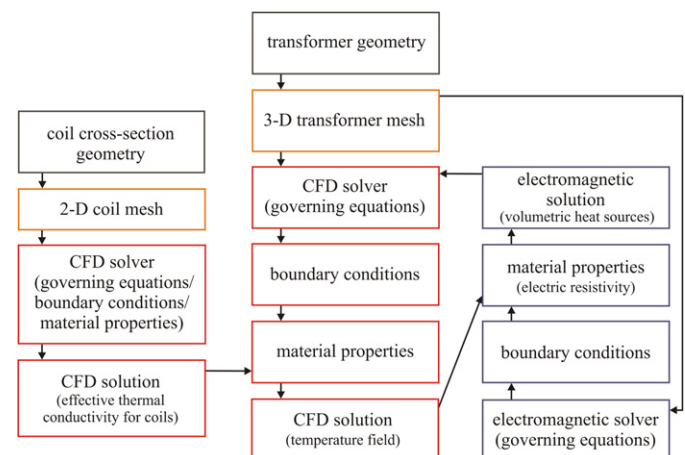

Fig. 1. Coupling scheme for the CFD-electromagnetic solutions.

3. Geometry and numerical mesh

In order to analyze the coupled thermal, fluid flow and electromagnetic processes taking place inside the transformer, a model of the geometry should contain not only the device itself, but also a transformer surrounding such as air, tank, radiators, cooling pipes, etc. Due to the complicated geometry of the transformer and its surrounding, all geometrical models created in this project were three-dimensional. Additionally, the investigated unit was a three-phase transformer which made the geometrical definition even more complex. Therefore, the geometry generation process, which is usually very time consuming, was performed using the commercial software Catia [17] and exchanged with a Fluent pre-processor Gambit via the ACIS (SAT) file.

The geometrical model was created on the basis of the technical documentation provided by a transformer manufacturer. Therefore, all device elements that were important to the investigated physical processes, such as the coils, core, core clampings, tank, cooler, etc. were maintained in their original shapes and dimensions. The overall geometrical dimensions of the 630 kVA transformer were: 1.36 m × 0.48 m × 1.37 m, see Fig. 2. The device was placed inside the transformer station that had dimensions 1.79 m × 0.81 m × 1.47 m, see Fig. 3. The tank and transformer were naturally cooled within only the surrounding air. Therefore, the characteristic features of both objects were taken into account in the geometrical model. To remove the heat from within the tank effectively, the natural convection on the external walls of the station was enhanced by twenty five flat fins welded to the top surface of the station, see Fig. 4. Additionally, the area of the side-walls of the station was increased by means of fifty cooling pipes (twenty five on each side), see also Fig. 4. The pipes were placed inside the tank such that both endings protruded from the station. However, the tank remained air and coal dust-tight. The cooling pipes were designed to work in the following way: the heat from the internal air is transferred to the external surfaces of the pipes. Then the heat is conducted through the pipe walls, and finally it is transferred from the internal pipe walls to the external air flowing through the pipes.

Both primary and secondary coils were naturally ventilated by means of the internal air. However, each of these coils was
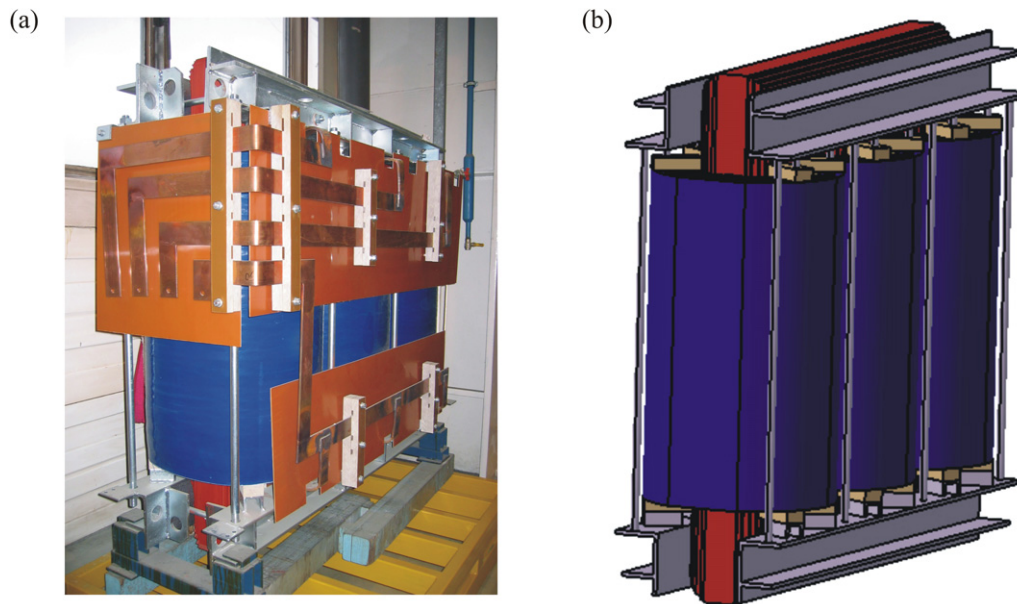

Fig. 2. The 630 kVA transformer working within the transformer station. (a) Photo, and (b) geometrical model (insulation shields not displayed here).
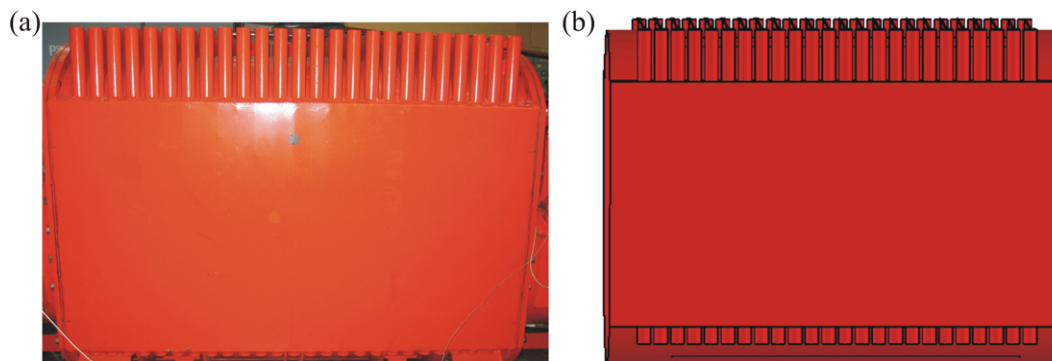

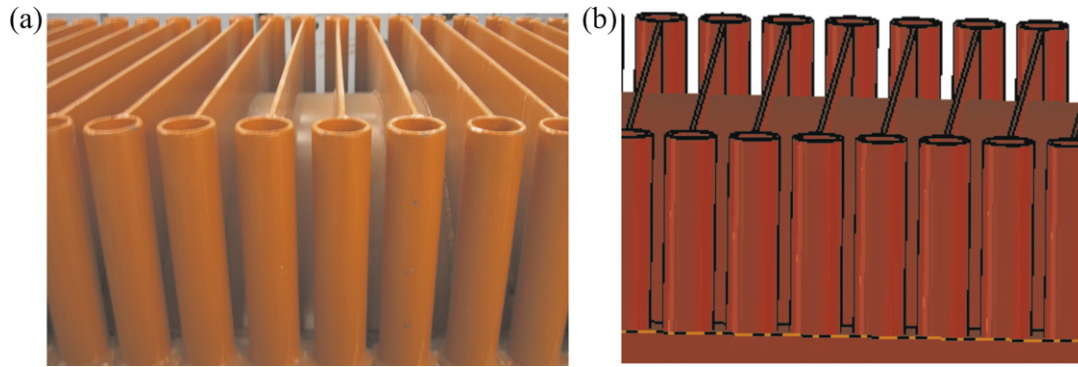Fig. 3. The tank of the 630 kVA transformer station. (a) Photo, and (b) geometrical model.

Fig. 4. The fins and the air cooling pipes welded to the tank of the 630 kVA transformer station. (a) Photo, and (b) geometrical model.
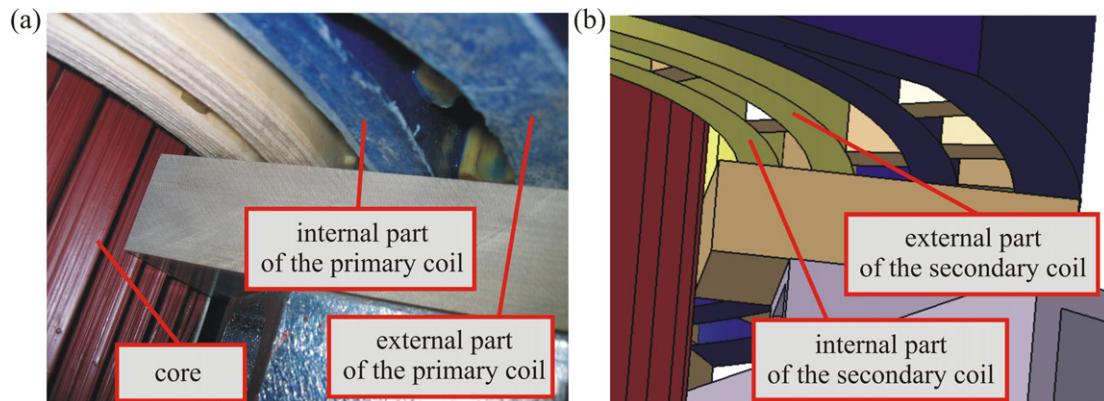

Fig. 5. Bottom view of the air ducts in the 630 kVA transformer. (a) Photo, and (b) geometrical model.

split into two parts. In this way, two additional air channels were obtained for the heat dissipation from the coils. This means that between the coils and core there were four air ducts around each of three core legs. Namely, the first duct was between the external and the internal parts of the primary coil. The second duct was between the internal part of the primary coil and the external part of the secondary coil. The third duct was between the external and the internal parts of the secondary coil. Finally, the fourth air channel was located between the internal part of the secondary coil and the core leg, see Fig. 5. In addition, the cross-section of the core leg in this transformer was not in the shape of a rectangle, as in typical solutions, but the cross-section was of a circles shape. Moreover, all the small elements in the coil locating pads were included in the model, see Figs. 5 and 6(a).

In general, a difficulty with the geometry creation for this model resulted from the several different scales. On one hand, the model had to consider such elements as the tank fins or the core clamping that were very thin (few millimeters), on the other hand, two of the tank overall dimensions exceeded 1.45 m. However, in this model it was possible to take advantage of a symmetry plane that cuts the core into two halves and was parallel to the side-walls of the tank. Therefore, only half of the real transformer station was geometrically modelled. To obtain the local heat fluxes on the interface between the transformer and the internal air within the station, between the internal air and the internal walls of the tank, and finally between the external walls of the tank and the external surrounding air,

both these air volumes were included in the geometrical model. The overall dimensions of the external air (and also the computational domain) were 2.29 m × 1.41 m × 1.67 m and these dimensions were based on the experience gained in the previous works by the authors [13,18,19].

During a simulation of the transformer performance, it was assumed that the coils could be represented by subdomains with an effective thermal conductivity varying with direction, as will be discussed in detail in the following section. To calculate the values of these material properties, both analytical and numerical analyses were used. In the case of the numerical models, two-dimensional cross-sections of the coils were considered. In such models an internal construction of the coil including wires, wire insulations, interlayer insulations, air gaps, etc. are taken into consideration. These elements were created and positioned on the basis of the information provided by the transformer manufacturer. Moreover, due to the different shapes and dimensions of the coil wires applied to the primary and secondary windings, their geometrical representations were generated and considered separately, see Fig. 6(b) and (c).

Both primary and secondary windings of the 630 kVA transformer were manufactured using two different techniques. The internal and the external parts of the primary coils were resin-immersed coils and consisted of flat wires, wire insulation and interlayer insulation, see Fig. 6. The applied cast resin as the interlayer insulation for the primary coils enables one to avoid any air gaps. The external part of the primary winding included 142 turns wound in 3 layers with the following dimensions of
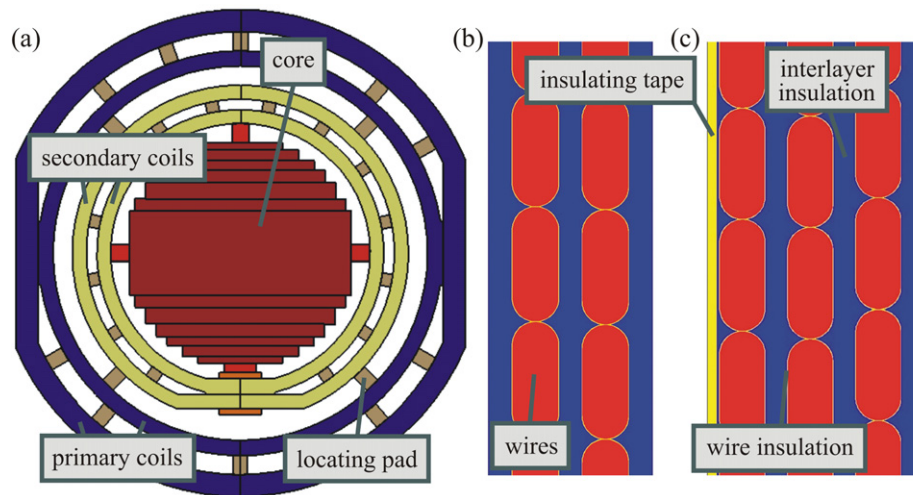
Fig. 6. Geometrical model of the coil cross-section of the 630 kVA transformer. (a) Top view of the primary and secondary coils and a cross-section of the core leg, (b) part of the internal primary coil cross-section, (c) part of the external primary coil cross-section.

the wire cross-section and a thickness of the wire insulation: 4.5 mm × 11.2 mm and 0.1 mm, respectively. The internal part of the primary winding included 124 turns wound in 2 layers with the following dimensions of the wire cross-section 4.5 mm × 11.2 mm. The wire insulation had a thickness of 0.1 mm. The overall dimensions of the external part of the primary coils cross-section were 16.2 mm × 790.0 mm, while those of the internal part were 22.2 mm × 790.0 mm.

Both parts of the secondary coils consisted of strip wires, insulation separating the wires and interlayer insulation. The external part of the secondary winding consisted of 25 layers with the following dimensions of the strip wire cross-section 0.4 mm × 350.0 mm and a thickness of the interlayer insulation 0.13 mm. The internal part of the secondary winding was wound in 24 layers with the following dimensions of the wire cross-section 0.4 mm × 350.0 mm. The interlayer insulation had a thickness of 0.13 mm. Each layer of both parts of the secondary coils included two wire strips that were placed one on the top of the other and separated from each other by insulating material. The overall dimensions of the external part of the secondary coils cross-section were 13.38 mm × 790.0 mm, while those of the internal part were 13.03 mm × 790.0 mm. However, all the coil elements were of rectangular shape and the effective thermal conductivity calculations were performed using analytical models. Therefore, geometrical models of the secondary coils were not required.

The generation of the fine mesh in the transformer geometry was complicated and required a high number of elements. Eventually, for the CFD computations, a mesh with 7.6 million elements was created. The numerical model with such a large mesh size was solved using parallel processing. Most solid elements of the transformer station (coils, a core, locating pads, a tank with the fins and the cooling pipes) were discretized with structural hexahedral elements only, see Figs. 7 and 8. In addition, the external air (not displayed in these figures) consisted of a very fine hexahedral mesh. The only geometrical elements containing a hybrid mesh were the clampings and partly the internal air in the vicinity of these elements.

The overall mesh quality generated within the 630 kVA transformer station was very high. According to the EquiAngle Skew and EquiSize Skew mesh quality-type specifications, more than 93% of the cells had a value less than or equal to 0.5 (classified as excellent and good elements). Additionally, taking into account the average mesh quality, the mesh had a value equal to 0.16, which was a far better value than recommended by Fluent for a high quality meshes, namely 0.4.

For the electromagnetic analysis, the geometrical model was simplified and included the coils, core, clampings, internal air and tank. Therefore, the mesh generated for this analysis was reduced and consisted of 1.1 million of elements. The quality of the generated grid was controlled in the same way as in the case described above. According to EquiAngle Skew, more than 91% of all mesh cells had a value less than or equal to 0.5, which means that the grid was of good quality.

4. Mathematical model

4.1. Governing equations for the CFD analysis

The steady-state temperature distribution within the device and its surroundings can be determined by solving the following energy equation (Fourier–Kirchhoff equation) [20]:

$$\nabla(k\nabla t) + q_v = \rho c \boldsymbol{w} \cdot \nabla t \tag{1}$$

where k is the thermal conductivity, t represents the temperature, q_v stands for the volumetric heat source, ρ is the density, c is the specific heat and w stands for the velocity vector.

The internal volumetric heat sources q_v in Eq. (1) were transformer losses occurring in the core and coils related to volumes of these transformer elements. To determine the values of the source terms in Eq. (1), an electromagnetic analysis has been performed. Such an analysis coupled with the CFD model produces temperature-dependent and local (in terms of space) results. The detailed information on the source calculations and the coupling procedure of the electromagnetic field with the main CFD analysis is given in the next subsection.
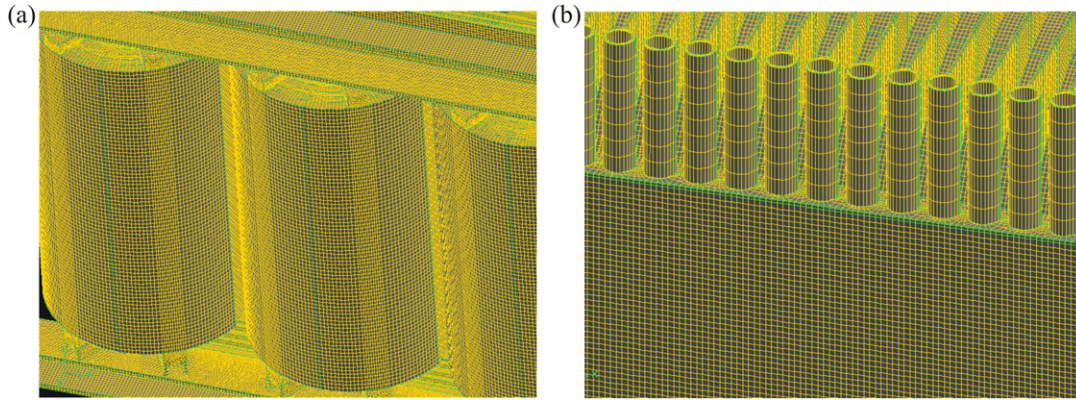
Fig. 7. Mesh generated within the 630 kVA transformer. (a) Side view of the coils and clampings, and (b) view of the fins and the cooling pipes of the transformer tank.
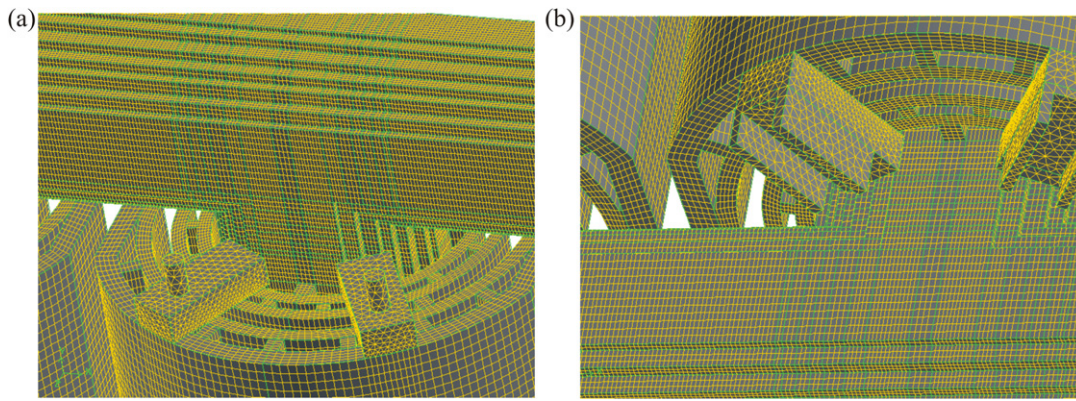

Fig. 8. Mesh generated within the 630 kVA transformer. (a) Top view of the core, coils, screws, and locating pads (mesh within the top clamping not displayed here) (b) bottom view of the core, coils and locating pads (mesh within the lower clamping not displayed here).

In the transformer standards and literature, the authors [14,20] distinguish between internal and external coolants. Transformer oil and air are the most popular internal coolants, while air and water are used in the external coolers. However, to describe a motion of any of these fluids, two types of equations should supplement the energy equation (Eq. (1)). These are the continuity and the momentum equations. Since in the project the air was considered as to be an incompressible Newtonian fluid, the continuity and the momentum equations take the following form, e.g. [21]:

$$\nabla \cdot \boldsymbol{w} = 0 \tag{2}$$

$$\rho \boldsymbol{w} \cdot \nabla \boldsymbol{w} = \boldsymbol{F} - \nabla p + \mu \nabla^2 \boldsymbol{w} \tag{3}$$

where $\boldsymbol{F}$ stands for the body force vector, p represents the pressure, while μ is the dynamic viscosity.

The motion of the internal and external air (inside and outside the transformer tank) was typical buoyancy-driven flow. Therefore, the above equations were supplemented with the relation describing the density variation:

$$\rho = \frac{p_{\text{op}}}{\frac{R}{M}(t + 273)} \tag{4}$$

where p_{op} represents the operating constant pressure (set to 0.1 MPa), R is the gas constant and M denotes the molar mass.

The preliminary results showed that a relatively high intensity of the turbulent flow occurred in the air flowing through the ducts between the coils, and between the coils and core, and also in the external air flowing around the external walls of the transformer tank. For this reason, for the turbulence modelling within this investigation, the standard $K-\varepsilon$ model was employed. This model is the most widely employed two-equation eddy-viscosity model [22]. Among its many applications, it has been successfully used for calculations of the air flow in longitudinal horizontal and vertical ducts [23,24] and for simulations of buoyancy driven flows in ducts [25] and enclosures [26]. The model is based on a solution of the following transport equations for the turbulent kinetic energy and the turbulent dissipation rate [22]:

$$pK\nabla \boldsymbol{w} = \nabla\left[\left(\mu + \frac{\mu_t}{\sigma_K}\right)\nabla K\right]$$
$$+ G_K + G_b - \rho\varepsilon - Y_M \tag{5}$$

$$\rho\varepsilon\nabla \boldsymbol{w} = \nabla\left[\left(\mu + \frac{\mu_t}{\sigma_\varepsilon}\right)\nabla\varepsilon\right]$$
$$+ C_{1\varepsilon}\frac{\varepsilon}{K}(G_K + C_{3\varepsilon}G_b) - C_{2\varepsilon}\rho\frac{\varepsilon^2}{K} \tag{6}$$

where K is the turbulent kinetic energy, μ_t stands for the turbulent dynamic viscosity, σ_K denotes the turbulent Prandtl number for K, ε represents the turbulent dissipation rate, σ_ε is the

turbulent Prandtl number for ε, G_K represents the generation of the turbulence kinetic energy due to the mean velocity gradients, G_b is the generation of the turbulence kinetic energy due to buoyancy, Y_M represents the contribution of the fluctuating dilatation in compressible turbulence to the overall dissipation rate, and finally $C_{1\varepsilon}$, $C_{2\varepsilon}$ and $C_{3\varepsilon}$ are constants depending on a variant of the $K-\varepsilon$ model.

The constants appearing in the model equations had the typical values taken from [27]. Since these constants have been determined from experiments with air and water for fundamental turbulent shear flows, the constants remained unchanged during all calculations in this investigation.

Apart from the heat conduction and convection, the third heat transfer mode, namely thermal radiation, is also considered in the mathematical model. Mathematically this phenomenon was divided into internal and external radiation. The internal radiative heat transfer occurred within the transformer tank filled with the cooling air, while the external radiative heat flux was exchanged between the external tank walls and the transformer surroundings.

The internal radiation was computationally much more complex than the external one and required an application of the radiation model. Among a number of the radiation models available in Fluent, within this project the Discrete Ordinate (DO) method has been selected. The DO model works well for complicated shapes for the computational domain. Moreover, it can be used for adapted meshes with hanging nodes and is compatible with parallel processing.

The DO radiation model solves the radiative transfer equation (RTE) for a finite number of discrete solid angles, each associated with a vector direction s fixed in the global Cartesian system. The implementation in Fluent uses a conservative variant of the discrete ordinate model called the finite-volume scheme [28], and its extension to unstructured meshes [29]. Thus, the DO model considers the RTE in the direction s as a field function:

$$\nabla \cdot \big(I(r,s)s\big) + (a + \sigma_s)I(r,s)$$
$$= an^2 \frac{\sigma(t+273)^4}{\pi} + \frac{\sigma_s}{4\pi} \int_0^{4\pi} I(r,s_s)\Phi(s,s_s)\,d\Omega \qquad (7)$$

where I is the radiation intensity, which depends on position r and direction s, r is the position vector, s stands for the direction vector, a is the absorption coefficient, σ_s is the scattering coefficient, n is the refractive index, σ is the Stefan–Boltzmann constant ($5.672 \times 10^{-8}\ \mathrm{W\,m^{-2}\,K^{-4}}$), t is the local temperature, Φ is the phase function, s_s is the scattering direction vector, and Ω is the solid angle.

The effectiveness of this method depends on the angular discretization and pixelation of the domain [29]. Within the work, the default values discretization of 2×2 and the pixel resolution of 3×3 (the default is 1×1) that is recommended for geometries with symmetry has been used. However, in the performed calculations it was assumed that the internal air was treated as a non-participating medium. Therefore, a simplified governing equation was considered for the radiative heat transfer between solids only, as in the Surface-to-Surface model.

The radiative heat transfer from the exterior of the transformer tank did not require activating any of the radiation models. The external radiative heat flux was calculated using the temperature difference of the tank wall t_w and internal walls of the surrounding room $t_{w,\infty}$. The following equation was used to calculate the total energy loss of the transformer tank due to radiation [30]:

$$Q_r = \sum_{i=1}^{n} A_i \sigma \varepsilon_w \big((t_{w,i} + 273)^4 - (t_{w,\infty} + 273)^4\big) \qquad (8)$$

where Q_r is the total heat transfer rate due to radiation from the tank wall, A represents the cell face area of the considered tank wall, σ stands for the Stefan–Boltzmann constant, ε_w is the emissivity, $t_{w,i}$ denotes the local temperature of the tank wall, $t_{w,\infty}$ stands for the wall temperature of surrounding room.

4.1.1. Local volumetric heat sources—coupling with electromagnetic field

In order to determine the source term q_v arising in Eq. (1), the analysis of the electromagnetic field was performed using a commercial package Ansys (EMAG module) that utilizes the Finite Element Method. The electromagnetic calculations resulted in a local distribution of the volumetric heat sources within the core and coils. In addition, this analysis required the coupling procedure between the thermal, fluid flow and electromagnetic solution due to the temperature-dependence of the electrical resistivity of the coils. From the mathematical point of view, the electromagnetic model constituted a part of the CFD computations. For this reason, the entire description of this model is presented in the following subsections.

The steady-state Maxwell equations [31], also known as Ampere's law, Faraday's law of induction, Gauss' law for magnetism and Gauss' law, respectively, need to be solved in order to obtain a solution of the coupled electromagnetic field. This set of equations is solved in Ansys by means of a magnetic vector potential approach. In this approach, Maxwell equations are simplified by omitting Gauss' law. Moreover, Ampere's law is written separately for the conducting part of the computational domain (Eqs. (9) and (10)), and for the non-permeable and the permeable, non-conducting parts of the computational domain (Eq. (11)). These equations can be expressed as [16,32]:

$$\nabla \times \frac{1}{\mu_c}\nabla \times A - \nabla\frac{1}{\mu_c}\nabla \cdot A + \frac{1}{\rho_c}\nabla V$$
$$- w_c \times \frac{1}{\rho_c}\nabla \times A = 0 \qquad (9)$$

$$\nabla \cdot \left(-\frac{1}{\rho_c}\nabla V_c + w_c \times \frac{1}{\rho_c}\nabla \times A\right) = 0 \qquad (10)$$

$$\nabla \times \frac{1}{\mu_c}\nabla \times A - \nabla\frac{1}{\mu_c}\nabla \cdot A = J_c \qquad (11)$$

The remaining equations for Faraday's law of induction and Gauss' law for magnetism can be written in this approach in the form [16,32]:

$$E_c = -\nabla V_c \qquad (12)$$
$$B = \nabla \times A \qquad (13)$$

where μ_c stands for the magnetic permeability, A denotes the magnetic vector potential, ρ_c indicates the electrical resistivity, V_c represents the electric scalar potential, w_c is the velocity vector of charge particles, J_c stands for the current density vector, E_c denotes electric field vector, B indicates magnetic flux vector.

The magnetic vector potential approach can be successfully applied to transformer-related problems [32] if the appropriate boundary conditions are introduced. In this study the boundary conditions of the first kind (Dirichlet) were prescribed on all external walls of the transformer tank:

$$A(x, y, z)|_S = A_S \tag{14}$$

where A_s is the component of the magnetic vector potential at the particular tank boundary. During all the electromagnetic simulations, the component of the magnetic vector potential A_s was explicitly set to zero. This means that the magnetic flux was parallel to each boundary S of the considered domain.

The above equations and boundary conditions have to be completed with adequate electromagnetic material properties. The properties defined for this analysis were: electrical resistivity and relative magnetic permeability. The electric resistivity for conducting material as coils was set as a temperature-dependent material according to the following linear relationship:

$$\rho_C = 1.709 \times 10^{-8} + 0.00393 \cdot (t - 20) \tag{15}$$

The relative magnetic permeability was treated as a constant for all materials. A value of this property for the transformer core was assumed to be 3000. Air and other materials, i.e. locating pads had the value of relative magnetic permeability equal to 1.

4.1.2. Solution strategy for the electromagnetic analysis—coupling with CFD

As stated in Section 3, all three-dimensional geometries and meshes of the considered transformers within tanks used in the electromagnetic calculation were generated in Gambit, a Fluent preprocessor [15]. Meshes were exported to a text file using the

export option for the Ansys solver. Then the mesh was automatically completed with an element type (related to an analysis type), boundary conditions and material properties by means of an in-house Fortran code. The model definition was prepared such that the file was read into the Ansys solver and run in a background mode without activating any other options or commands.

Apart from the 3-D numerical models of the considered three-phase transformer, a three-phase electric circuit was appended in order to analyze devices under different loadings, see Fig. 9. Since the windings of the analyzed transformer were connected in Yy configuration, this type of the circuit connection was modelled. In general, such a circuit consisted of three independent voltage sources (IVS), three load resistors (R), three internal resistors (IR) and twelve 3D stranded coils (SC). The circuit was connected to the three-dimensional domain by means of stranded coil circuit elements. It required a coupling of the electric current and the electromotive force of the coils in the numerical model. Furthermore, in these elements the basic parameters of the real coils were defined such as the coil cross-sectional area, total number of coil turns x-, y- and z-components of a unit vector (in the element coordinate system) representing the direction of the current, and coil volume.

Such a configuration for the circuit is universal because the independent voltage sources in this circuit could be used to set the arbitrary phase voltages and angles. Additionally, different values of the electric resistance in the secondary circuit elements allowed one to carry out the transformer simulations under different power conditions, i.e. the short-circuit test, open-circuit test, underloading, overloading and under nominal parameters.

The temperature-dependent resistivity required a coupling of the electromagnetic and CFD solutions through an iterative process. Namely, the heterogeneous temperature field in the coils was used to define a new set of local electrical properties for the coils applied in the electromagnetic model. Then the electromagnetic simulation determined the local heat losses
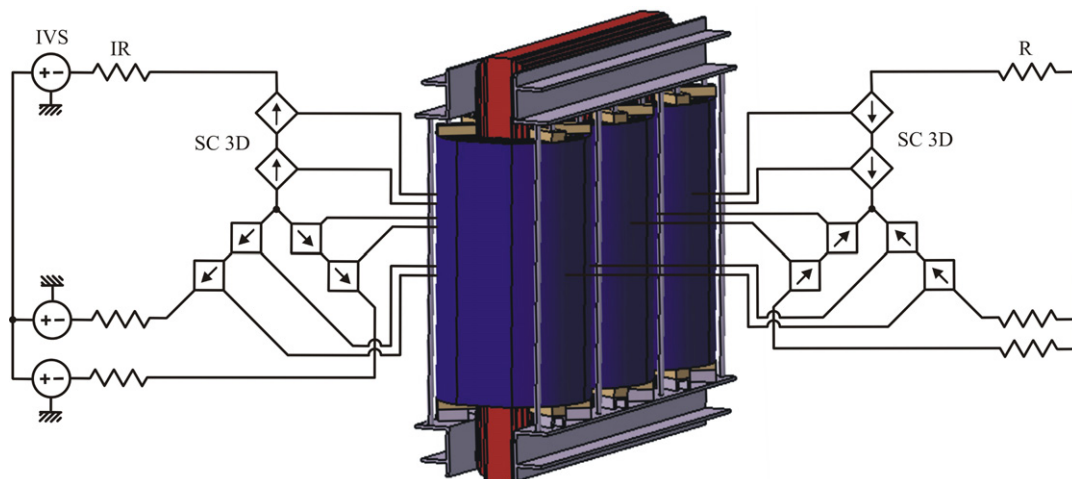

Fig. 9. Electric circuit for the electromagnetic calculations. IVS—independent voltage source, IR—internal resistor, SC 3D—stranded coil, R—load resistor.

in the windings (the Joule losses) according to the following formula:

$$q_v = \frac{1}{2}|\boldsymbol{J}_{c,\max}|^2 \rho_c \qquad (16)$$

where $\boldsymbol{J}_{c,\max}$ denotes the maximum current density vector.

Calculations of the transformer core energy losses required two steps: first, Ansys Emag produced the field of a magnetic flux in each mesh element of the core and these values were next used to define a curve of the specific power loss in $\mathrm{W\,m^{-3}}$ as a function of the maximum magnetic flux and current frequency [33]. This procedure resulted in the following relationship, known as the Steinmetz equation:

$$q_v = m_{\mathrm{St}} f B_{\max}^{n_{\mathrm{St}}} \qquad (17)$$

where f is the current frequency, $B_{\max}$ stands for the maximum magnetic flux, m_{St} and n_{St} represent the coefficient and the exponent of Steinmetz equation.

The value of the exponent n_{St}, as usually referenced in literature [34], is equal to 2.5, while the coefficient n_{St} depends on a few physical quantities, e.g. core geometry. The value of this coefficient is determined on the basis of the calculations and experiments. Since the total core loss was obtained from the experimental tests in an open-circuit, its value and the value of the core volume were used to specify the coefficient by summing up all the local losses (in each grid element) according to Eq. (17).

All the volumetric heat sources calculated utilizing Ansys Emag were interpolated and then implemented (using User Defined Functions [15]) into the finer mesh in the Fluent solver.

4.2. Local heat fluxes as boundary conditions for the CFD analysis

To determine the temperature distribution within the transformer and the surrounding air, it was necessary to complete the governing equations for the CFD model with appropriate boundary conditions and material properties. As the transformer and the standard heat transfer literature reports, the boundary conditions can be determined in many ways. There are a number of papers, [6,7], in which the authors have calculated the values of the heat transfer coefficients based on the averaged Nusselt number equations. More advanced approaches specify them as temperature-dependent values. However, both these analyses take into account only the average wall temperature. Another way of prescribing the boundary conditions is using measurement data. To obtain this information, many measurement techniques can be employed. When thermocouples are used, the resulted temperature field is obtained at selected points. This information can be used to compute the average boundary temperature or to prescribe a simplified temperature distribution on only a certain wall. Better results can be obtained by means of infrared thermography [35,36]. However, an interpretation of the results for the complicated shapes of the surfaces, e.g. a tank with the convex top wall with fins and cooling pipes on it, is complicated. Moreover, such measurements can be performed for only the visible surfaces. For this

reason, within this project the boundary conditions based on the CFD analysis of the air surrounding the modelled transformer and the tank were determined. In this way the prescribed boundary conditions were the local and temperature-dependent heat fluxes. The implemented approach for the determination of the boundary condition was validated independently using thermocouples and also infrared thermography. Furthermore, the performed analysis provided information on the heat transfer coefficient distribution and its average values for the investigated unit. These results can be used in a simplified analysis of the heat conduction processes taking place within transformer elements.

In the analysis, the transformer with the surrounding air within the tank (internal air), the tank, and the air surrounding the tank (external air) were considered as a single domain. Therefore, the boundary conditions need to be specified on the exterior of the external air. The dimensions of the domain were taken to be sufficiently large to ensure that the thermal and flow conditions of the calm ambient air (geometrically modeled as a brick) on the external boundary are accurately modelled. Moreover, it was expected that the heated air would mainly flow out of the domain through its top wall and the cold air would flow into the domain to fulfill the mass conservation law. To achieve this, the pressure outlet boundary conditions were prescribed on all the external walls of the surrounding air. This is a typical boundary condition type for flows that can reverse direction near a boundary. It required the specification of the static pressure and temperature of the backflow at the outlet boundary. Since all reported calculations refer to experiments performed in large rooms, these parameters were set to the atmospheric pressure ($p = 101\,325$ Pa) and the ambient air temperature of the room $t_\infty = 18\,°\mathrm{C}$, respectively. All other flow quantities were extrapolated from the interior values.

4.3. Material properties for the CFD analysis

Apart from boundary conditions, the governing equations presented in Section 4.1 had to be completed with appropriate material properties. Since all calculations were carried out in steady-state, the only material property for the solids that occurred in the Fourier–Kirchhoff equation for such a process was the thermal conductivity. In addition, because of the presence of radiation, the emissivity also entered the analysis. The material properties for solids were measured, provided by manufacturers or gathered from the standard literature [20,30]. The values of the thermal conductivity and the emissivity defined in the CFD calculations are listed in Table 1.

4.3.1. Anisotropic thermal material properties for coils and core

Due to the complex construction of the coils and the core, anisotropic material properties for these elements were defined. Results of such an approach show that this procedure appears to be much more accurate when compared to using a simplified model of the isotropic material properties for the coil and the core based only on the engineer's intuition [18]. As shown in Fig. 10(b), typical coil elements that should be taken into con-
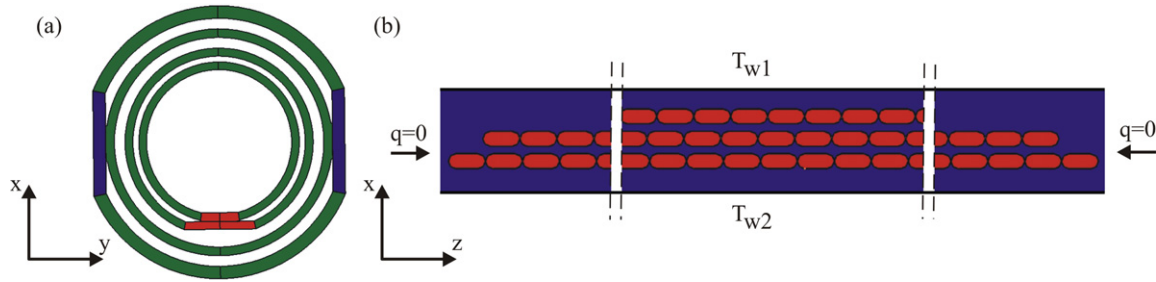
Fig. 10. (a) Geometry of coils. Gray-scale colours in this figure denote regions with different type or alignment of the coordinate system, and (b) cross-section of the exemplary coil with the prescribed boundary conditions.

Table 1
Thermal material properties for solids

Transformer element	Thermal conductivity, $W\,m^{-1}\,K^{-1}$	Emissivity
copper for wires	385	–
wire insulating materials	0.2	0.95
coil interlayer materials	0.13	0.95
steel sheets for core	40	–
steel sheets coating	0.44	0.93
carbon steel for cooling coil, tank, clampings, screws	0.35	0.98 (measured for the tank paint by an infrared camera)
insulating material for locating pads	0.57	0.95
bakelite for insulation shields	0.23	0.85

sideration are: wire, wire insulation and interlayer insulation. As regards the core, the transformer element consisted of insulated laminates. In this study, it was assumed that both the coil and core behave like a homogenous material and have only one equivalent (effective) value [12] for the thermal conductivity in each coordinate direction.

In order to calculate the equivalent thermal properties for the coil, a few geometrical regions in this transformer element had to be distinguished, see Fig. 10(a). These were the corners and rounded parts of the coils, and the straight parts of the coil. In all these subregions the same three thermal conductivities k_i, k_j and k_k were specified, but these values were applied for different directions and/or coordinate system types. Namely, a Cartesian coordinate system was defined in the straight parts of the wires that are aligned to global coordinate system, while cylindrical coordinates were employed in rounded parts of the coil. However, for certain coil parts, a local rectangular coordinate system was rotated with regards to the global coordinate system. Furthermore, the effective values of the thermal conductivity were determined in two different ways: a numerical conduction model was used for the two cross-sectional directions to the wires [11,12], while an analytical model was employed for the direction along the wires.

In order to determine the anisotropic thermal conductivities for the cross-sectional direction to the wires, 2-D numerical models of the cross-section of each coil were built up. The primary and secondary windings consisted of internal and external parts. However, only for the primary coils, two models of both parts were analyzed. The effective thermal conductivities for both parts of the secondary coils were calculated using analytical models.

For each type of the coil, two tests were carried out in order to determine the thermal conductivities in two perpendicular directions. In the 2-D models, conduction occurred in the wires and the insulation materials were considered to be isotropic. Hence, to calculate the effective thermal conductivity in the vertical direction, the boundary conditions in the numerical model, see Fig. 10(b), were prescribed as follows: two vertical parallel walls were insulated (no heat flux flowed through the boundary), while on the other horizontal parallel walls, the Dirichlet (known temperature) boundary conditions were specified.

From these calculations, the average heat flux flowing through the cross-section of the coils was obtained. Then the effective thermal conductivity in the ith direction (x in Fig. 10(b)) is computed from the following equation (Fourier law) [20]:

$$q_i = -k_{i,\text{eff}}\frac{\partial t}{\partial i} \tag{18}$$

where q_i is the heat flux in the ith direction, $k_{i,\text{eff}}$ is the effective thermal conductivity in the ith direction.

In the case of the thermal conductivity in the direction along the wires, analytical models were utilized for all coils. Namely, an analogy of electrical resistivities connected in parallel was used to compute the effective value of this property. For this reason, the following relationship may be used for the ith direction:

$$k_{i,\text{eff}} = L_i \sum_{j=1}^{n} \frac{k_j}{L_j} \tag{19}$$

where L_i stands for the length of the coil wire in the ith direction, k_j is the thermal conductivity of the jth material in the coil, while L_j represents the length of the jth material layer in the coil in the ith direction.

However, in the perpendicular direction to the strip wires of 630 kVA transformer coil the following formula for a series connection of the resistivities was used:

$$k_{i,\text{eff}} = \frac{L_i}{\sum_{j=1}^{n} \frac{k_j}{L_j}} \tag{20}$$

The values of the effective anisotropic thermal conductivities obtained from both numerical calculations and analytical models are listed in Table 2. In general, these values were lower by two orders of magnitude compared with pure those for the copper used for coil wires.

Table 2
Effective anisotropic thermal conductivity (in $W\,m^{-1}\,K^{-1}$) for the coils in the 630 kVA transformer. Two values in each direction were obtained for the internal and external coils, respectively

Primary coil			Secondary coil		
$k_x = k_r$	$k_y = k_\varphi$	k_z	$k_x = k_r$	$k_y = k_\varphi$	k_z
0.98/0.99	146.5/156.3	2.30/2.64	1.89/1.97	287.4/291.6	287.4/291.6

The considered core consisted of flat steel laminates separated from each other by a layer of varnish. Hence, in the case of the core, the thermal conductivity in each direction was computed using again the analytical models. Its effective value was considered as a connection of parallel resistivities for two parallel directions to laminates, while the formula for a series connection of the resistivities was used for the perpendicular direction to the laminates, see Eqs. (23) and (24), respectively. As a result of these calculations, the following values were obtained for the core: $k_x = k_z = 48.9\,W\,m^{-1}\,K^{-1}$ for the two directions in the laminate plane, and $k_y = 14.5\,W\,m^{-1}\,K^{-1}$ for the perpendicular direction to the laminates.

The coolants used within the considered transformer cases were the internal and external air. To solve the CFD equations, the following material properties were required for the fluids: density, specific heat, thermal conductivity and dynamic viscosity. To model the buoyancy driven flow of these agents, special attention was paid to the modelling of the air density. Namely, an incompressible ideal gas law for the density variations (due to significant temperature differences in the Boussinesq model was not employed) was used. The remaining properties for the coolants were defined as temperature-dependent values using polynomial functions in the temperature range obtained from the experimental measurements [20,30].

5. Validation of the numerical model

In the literature regarding the numerical analysis, there are many definitions of numerical model validation. The authors of [37] stated that validation is the process of determining the degree to which a model is an accurate representation of the real world from the perspective of the intended use of the model. In this paper, the temperature rise tests of the considered transformer were utilized to validate the numerical simulations. The temperature values were captured by means of thermocouples, thermometers, pyrometers and infrared thermography.

5.1. Procedure for the experimental measurements

To perform the temperature rise test, two following loading methods can be applied according to the European Standards at the choice of the manufacturer [14]: the direct loading method and the back-to-back method. For the 1 kVA transformer analyzed in [13], the direct loading method was used. In this method, one winding, preferably the inner winding, of the transformer is excited at the nominal voltage with the other connected to a suitable load such that the nominal currents flow in both windings. However, as it was performed for the 630 kVA

transformer, by agreement between a manufacturer and a purchaser, a simulated load method can also be applied [14]. The temperature tests are made by utilizing the rises obtained from the two tests, one with no load loss only, and one with load losses only, i.e. the open- and short-circuit run. The no-load test, at a nominal voltage, was continued until the steady-state conditions were obtained. Then the individual winding temperature rises, Δt_e, were measured. The short-circuit run with a nominal current flowing in one winding and the other winding short-circuited was started immediately following the no-load run, and continued until the steady-state conditions were obtained and the individual winding temperature rises Δt_c were measured.

Then on the basis of the obtained winding temperature rises Δt_e and Δt_c, the total winding rise Δt of each winding with a nominal current in the winding and normal excitation of the core was calculated using following formula:

$$\Delta t = \Delta t_c \left[1 + \left(\frac{\Delta t_e}{\Delta t_c} \right)^{1.25} \right]^{0.8} \tag{21}$$

where Δt denotes the total winding temperature rise, while Δt_e and Δt_c represent the winding temperature rises in the open-circuit and short-circuit runs, respectively.

The ultimate temperature rise was reached when the temperature rise became constant. This was considered to be achieved when the temperature rise does not vary by more than 2% of the permissible rise per hour or 2 °C per hour, whichever is the smaller. Moreover, according to the Standard, thermocouples or thermometers should be applied for the sealed units at the centre of the top cover surface and at the centre of one side of the enclosure surface in order to determine when the temperature rise becomes constant.

By means of the simulated load method, the average winding temperatures were determined by winding resistance measurements [38]. In the case of three-phase transformers, it is recommended to perform these tests for the coil wound around the central core leg. The first measurement of the winding resistance $R_{c,a}$ was made at the known reference temperature t_a in steady-state conditions, while the second one was at the end of the temperature test to obtain the winding resistance R_c at a different temperature t. The following relationship was used to calculate the average copper winding temperature utilizing the measured resistances $R_{c,a}$ and R_c:

$$t = \frac{R_c}{R_{c,a}}(235 + t_a) - 235 \tag{22}$$

where $R_{c,a}$ and R_c stand for the winding resistances measured at reference and steady-state winding temperatures, respectively.

Results of the temperature tests for a particular transformer have been presented in comparison with the numerical ones in the following sections.

5.2. Comparison of the experimental and computational results for different device loads

The investigated unit was a three-phase Yy device positioned vertically and operated under the following nominal pa-
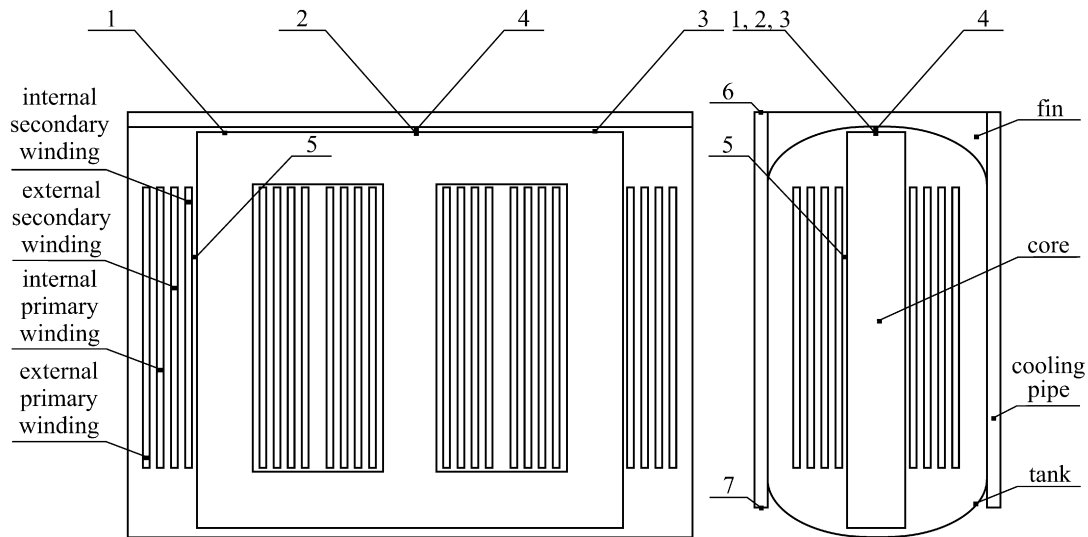
Fig. 11. Schematic layout of the thermocouples and thermometer locations within the transformer station. Temperatures at these points are listed in Table 3.

Table 3
Temperature values (in °C) within the transformer obtained in the open-circuit and short-circuit tests

Measurement point	Temperatures in open-circuit		Temperatures in short-circuit	
	Measured	Calculated	Measured	Calculated
1	95	95	93	100
2	103	98	95	99
3	98	96	93	98
4	58	52	80	79
5	73	73	114	117
6	28	31	21	24
7	18	18	18	18
8	33	39	56	60
9	27	31	46	50
10	41	46	49	49
11	35	41	55	65

rameters [39]: voltages PRI—$U = 3 \times 6000$ V, SEC—$U = 3 \times 1050$ V, frequency $f = 50$ Hz, current $I_c = 346.4$ A, power $P = 630$ kVA, coil and core losses, $\Delta P_{\mathrm{Cu}} = 3800$ W and $\Delta P_{\mathrm{Fe}} = 1800$ W, respectively. During the temperature test, the temperature field was monitored by means of five thermocouples mounted within the transformer tank. The sensors measured temperatures on the top surface of the core above each leg, the air between the core and the top wall of the tank, and the air in the duct between a left core leg and the secondary internal coil (points 1–5 in Fig. 11 and in Table 3). Moreover, the thermometers captured the temperatures of the air at the inlet and the outlet of the central cooling pipe (points 6–7 in Fig. 11 and in Table 3). Additionally, the temperatures of the external surfaces of the transformer tank were also monitored by means of infrared thermography.

In the temperature test on the transformer, a simulated load method was utilized. Therefore, a comparison between the experimental and computational results was made separately for the open-circuit and short-circuit tests. Furthermore, using the results of the resistance measurements of the windings, the average winding temperature was determined. These values were

also compared with computations from the CFD model of the transformer running under the nominal parameters.

To simulate a no-load run of the investigated device, all three load resistors in the transformer circuit (see Fig. 9) were set to very high values. As a result of these calculations, the heat source for the core was determined in the range of 2.3 W m^{-3} to 280 kW m^{-3}, see Fig. 12. The average value of a source term was about 102.5 kW m^{-3}. Using these losses, the final temperature field was determined for the open-circuit test, see Fig. 13. Since only the core generated heat, this element had the highest temperature. In addition, large differences along the height of the core can be observed. Moreover, the most effective heat removal from the core was under and above the coils. This resulted in higher temperatures in the air ducts, especially in the central core leg.

The results obtained from the computations were also compared with data captured during the experimental test in the open-circuit, see Table 3. The accuracy of the obtained temperatures was very satisfactory for both the external and internal temperature sensors.

In the post-processing analysis, the values of the temperature were compared with the measurement data not only at selected points where the thermocouples were mounted, but also the entire field of the external tank walls was validated, see Figs. 14(a) and 15(a). This comparison also turned out to be very accurate. The shape of the isotherms at the top and the side external wall of the tank corresponded to the infrared photos. Additionally, the hot spots that occurred at the walls of the tank were correctly identified. Further, the values of the calculated temperature were very similar to those obtained from the infrared measurements, see rows 8–11 in Table 3. The location of these sample points is presented in Figs. 14 and 15. The discrepancy in the results did not exceed about 6 °C, while the smallest difference was only 4 °C.

In the analysis of the temperature test in the short-circuit, all three load resistors in the transformer circuit (see Fig. 9) were set to almost zero to simulate a short-circuited run of the considered device. As a result of these calculations, the heat sources
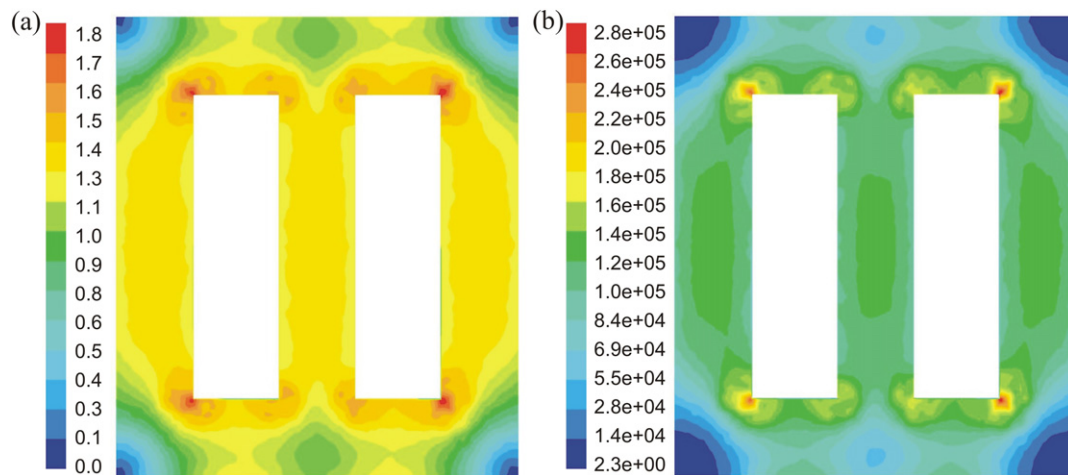
Fig. 12. (a) Distribution of maximum magnetic flux (in T), and (b) internal heat sources (in W m^{-3}), in the transformer core (longitudinal cross-sectional views).

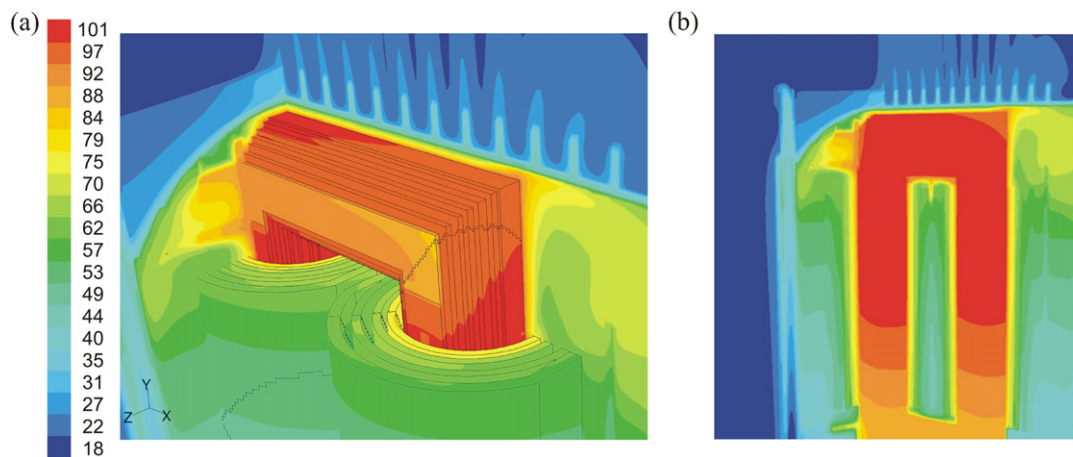Fig. 13. Temperature fields (in °C) within the transformer station running in the open-circuit test. (a) View of the central and the right coils, core and two cross-sectional planes, and (b) cross-sectional view of the core and other parts of the transformer station.
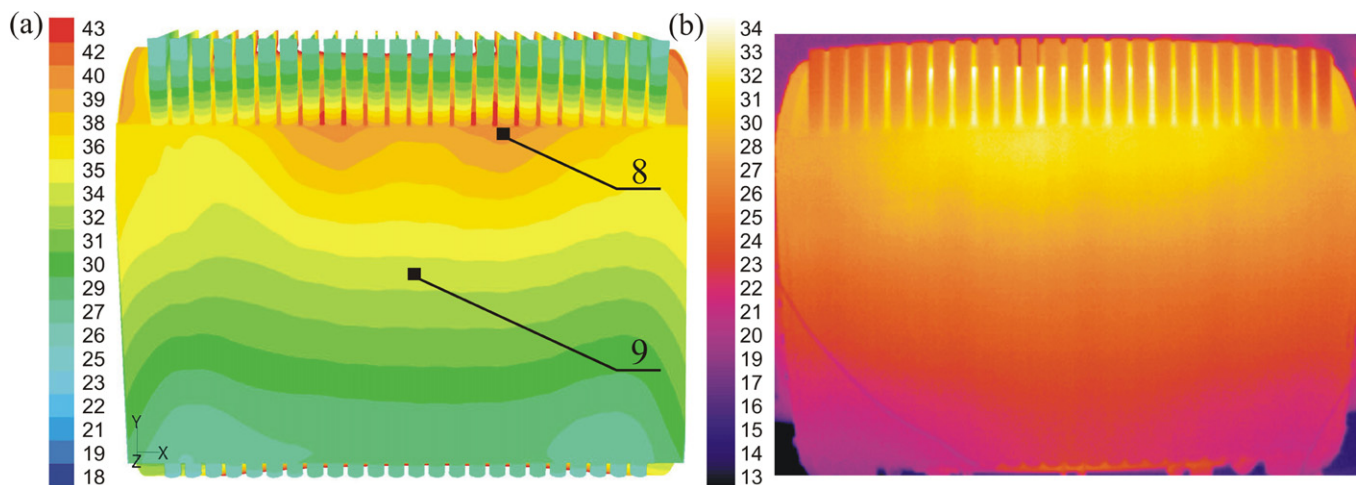

Fig. 14. Temperature field (in °C) on the external side tank walls of the transformer station running in the open-circuit test. Temperatures from (a) computational test, and (b) infrared camera. Temperatures at the indicated points are listed in Table 3.
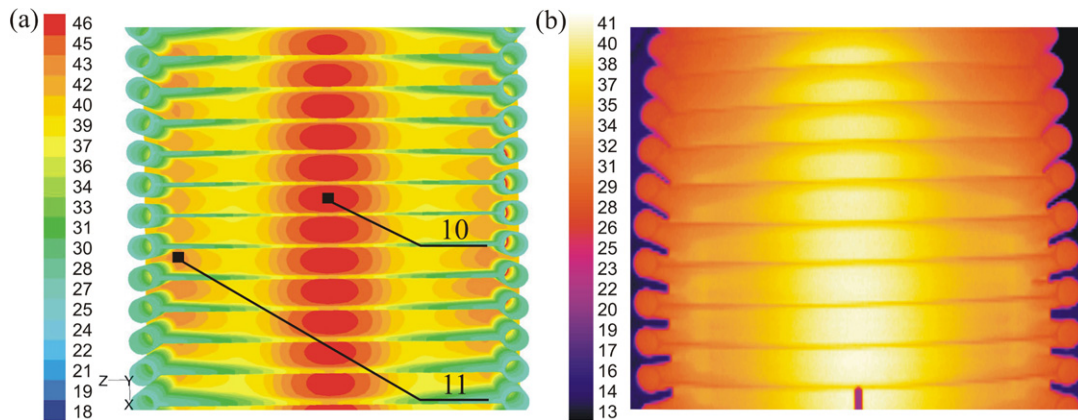
Fig. 15. Temperature field (in °C) on the external top tank walls of the transformer station running in the open-circuit test. Temperatures from (a) computational test and (b) infrared camera. Temperatures at the indicated points are listed in Table 3.
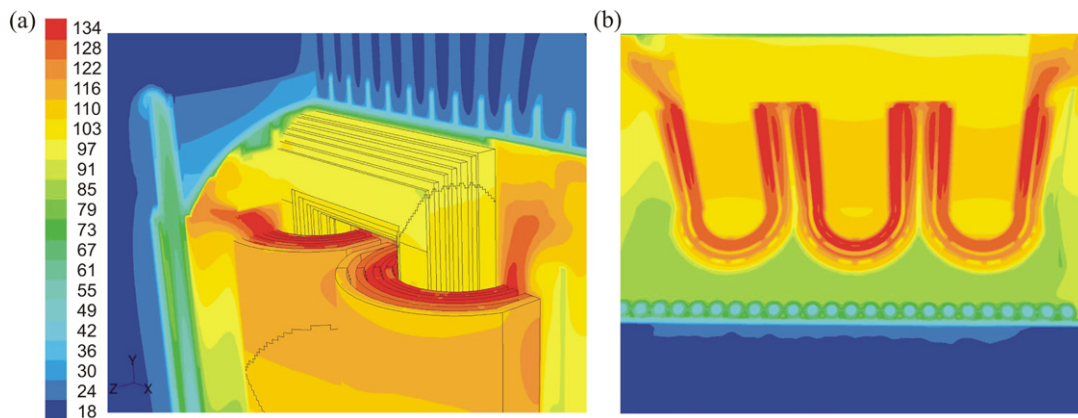

Fig. 16. Temperature fields (in °C) within the transformer station running in the short-circuit test. (a) View of the central and the right coils, core and two cross-sectional planes, and (b) cross-sectional view of the core and other parts of the transformer station.

for the coils were determined in the range of 13.8 $\mathrm{W\,m^{-3}}$ to 37.8 $\mathrm{W\,m^{-3}}$. On the basis of these losses, the final temperature field was determined for the short-circuit test, see Fig. 16. Since only the coils generated heat, these elements had a far higher temperature than the other elements, e.g. the core. However, the secondary coils were significantly warmer than the primary coils, see Fig. 16(b). In these figures it can also be observed that the hot air flows out from the air ducts.

As in the open-circuit test, the results obtained from the computations were also compared with data captured during the experimental test in the short-circuit, see Table 3. The accuracy of the obtained temperatures was even more satisfactory than in the open-circuit test for both the external and internal temperature sensors. The largest temperature difference was only 7 °C and in the case of points 4–7 was less than 3 °C.

The numerical model was also validated by means of the infrared camera, see Figs. 17 and 18. The comparison of the isotherm shapes on external top and side external walls of the tank with the infrared photos turned out to be very accurate. Additionally, the prediction of the hot spots that occurred in the presented walls of the tank was correctly identified. Furthermore, the values of the calculated temperature were very similar to those obtained from the infrared measurements, see

rows 8–11 in Table 3. The location of these sample points was the same as in the open-circuit analysis and, therefore, was presented in Figs. 14 and 15. The discrepancy in the results did not exceed 10 °C, while in the case of the point 10, the temperature was predicted with no error.

During both the short-circuit and open-circuit tests, the winding resistances were measured to calculate the average winding temperatures according to Eq. (26). These measurements were performed for the primary and secondary coils wound around the central leg of the core. Then on the basis of the temperature rises obtained in both tests, the total temperature rise corresponding to nominal parameters load was determined utilizing Eq. (25). To compare these values with the computational results, the CFD analysis of the transformer running under the nominal parameters was performed. The obtained temperature field from all three tests showed a good agreement with the computational predictions, see Table 4. Moreover, in this table the maximum winding temperatures were presented for the investigated cases, which significantly differ from their average values. A cross-sectional view of the entire temperature field in the analyzed windings and other elements of the transformer station can be seen in Fig. 19.
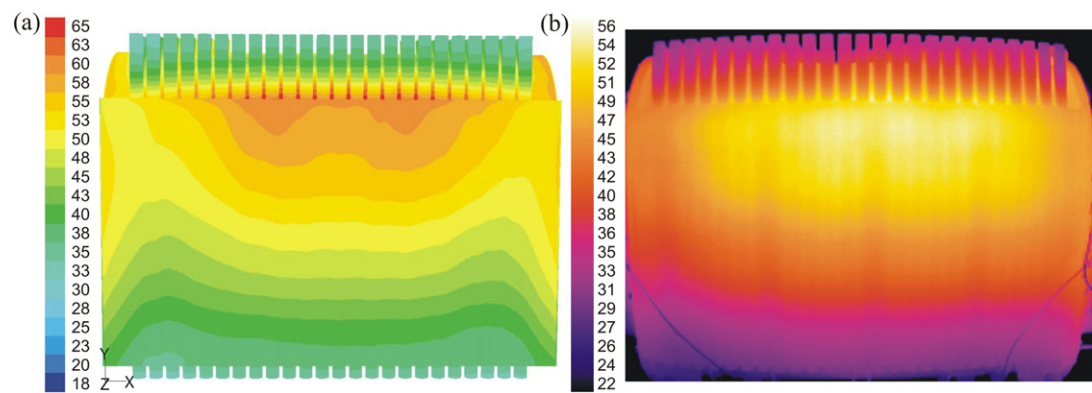
Fig. 17. Temperature field (in °C) of the external top tank walls of the transformer station running in the short-circuit test. Temperatures from (a) computational test and (b) infrared camera.
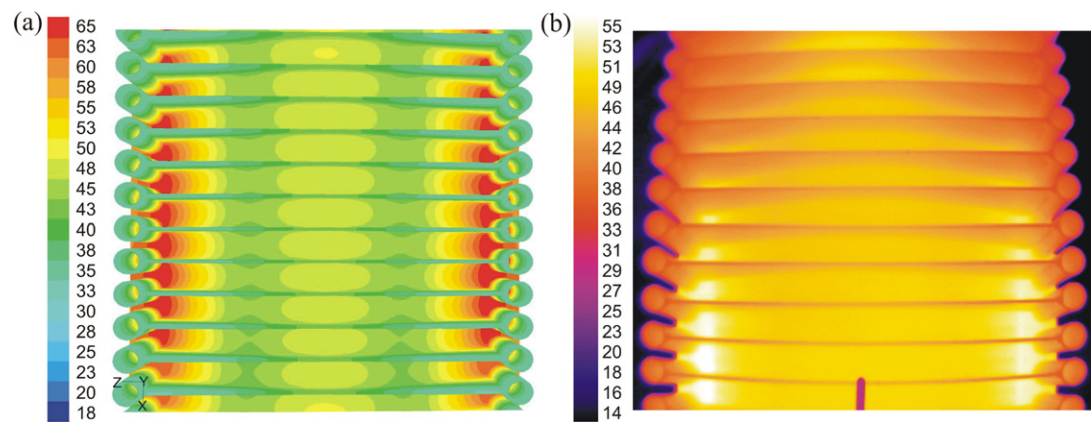

Fig. 18. Temperature field (in °C) of the external top tank walls of the transformer station running in the short-circuit test. Temperatures from (a) computational test and (b) infrared camera.

Table 4
Average and maximum temperatures (in °C) of the windings of the transformer station running in the open-circuit, short-circuit and under a simulated nominal load

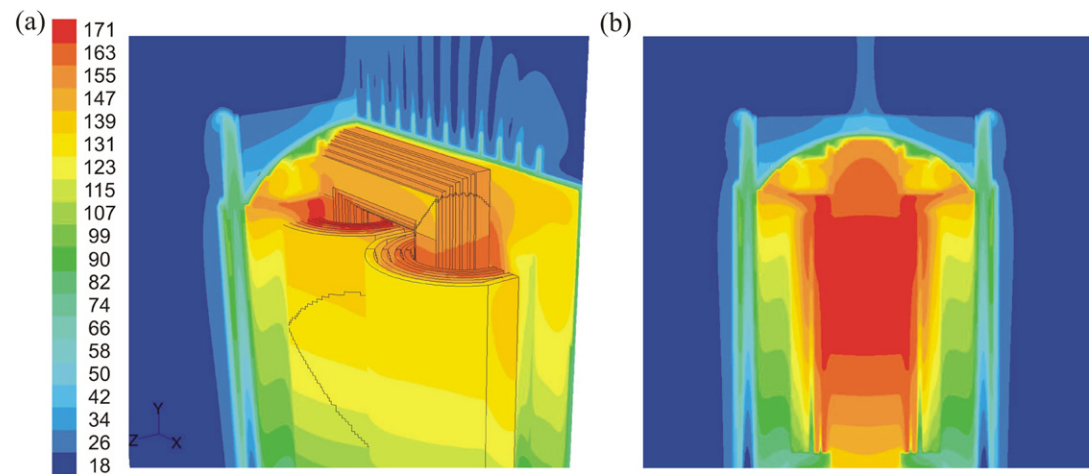| Test	Measured average temp.		Calculated average temp.		Calculated max temp.	
	PRI coil	SEC coil	PRI coil	SEC coil	PRI coil	SEC coil
Open-circuit	39.0	51.4	52.6	68.5	64.7	72.9
Short-circuit	116.4	123.8	110.8	127.9	133.1	134.3
Rated load	127.1	142.8	131.8	160.6	157.9	168.2

Fig. 19. Temperature fields (in °C) within the transformer station running under nominal parameters. (a) View of the central and the right coils, core and two cross-sectional planes, and (b) cross-sectional view of the core and other parts of the transformer station.

Table 5
Maximum temperatures (in °C) of the central coils and core of the transformer running under the nominal load

Element name	Maximum temperature	
	without radiation	with radiation
Internal secondary coils	219.4	170.8
External secondary coils	214.2	164.8
Internal primary coils	212.8	159.1
External primary coils	211.7	156.2
Core	203.3	169.1

5.3. Heat transfer modes in the dry-type transformer

To investigate the influence of the radiation on the temperature field within the device, in one of the computational runs the internal and the external radiative heat transfer was neglected. The results listed in Table 5 indicated very large increases in the maximum temperatures for particular coils and also the core. Namely, the smallest difference was 34.4 °C, while the largest was even 55.5 °C. Therefore, in the computations of the dry-type transformers, thermal radiation cannot be neglected.

Interesting results were also obtained for the case in which the transformer was insulated from the tank. As a result, the transformer dissipated heat via convection and radiation only (the heat was not conducted to the tank). The obtained increase in the maximum temperature was only 3 °C. This means that the heat conduction to the transformer tank did not noticeably improve the heat dissipation.

It appears that for the existing transformer construction, that the performance of the heat removal could be achieved by optimization of the fins and cooling pipes attached to the transformer tank.

5.4. Average total heat transfer coefficients

In the transformer literature, there are a number of works, in which the fluid flow surrounding the transformer is not considered. In such simplified analyses of the heat conduction processes, appropriate boundary conditions are required. Therefore, in this subsection the total average heat transfer coefficients (sum of the convective and radiative coefficients) were presented. Values of the heat transfer coefficients listed in Table 6 were taken from the tests presented in the previous subsections. This means that data were obtained for the 630 kVA unit working in the open-circuit, short-circuit and also under the nominal parameters.

It was assumed that the total effective heat transfer coefficients were calculated on the basis of the average total heat flux and the absolute difference between the average wall and air temperatures. The average values of the heat flux and wall temperature originated from their local distributions on the external boundaries of the particular transformer element. However, during the coefficient computations for the external tank walls, the average air temperatures were defined as the temperatures in the large room $t_{air,int}$, while for all the walls within the tank, the heat transfer coefficients were obtained taking the average temperature of the internal air $t_{air,\infty}$ into account. Therefore,

Table 6
The average heat transfer coefficients (in $W\,m^{-2}\,K^{-1}$) for the main transformer elements for the considered unit running in the open-circuit, short-circuit, and under the nominal parameters

Element name	Open-circuit	Short-circuit	Rated param.
Internal walls	$t_{air,int} = 51\,°C$	$t_{air,int} = 87\,°C$	$t_{air,int} = 121\,°C$
Central PRI coil	7.4/3.6	8.1/4.1	23.8/5.1
Central SEC coil	1.5/0.7	5.2/5.9	6.0/5.2
Side PRI coil	6.3/5.4	10.1/4.6	39.0/5.9
Side SEC coil	2.1/0.5	5.2/5.9	7.1/5.8
Core	5.1	1.4	11.5
Top clamping	5.9	37.1	48.5
Bottom clamping	4.9	11.8	21.2
Tank top wall	46.1	94	77.7
Tank side walls	16.7	19.8	12.1
Tank bottom wall	6.4	3.7	4.3
Cooling pipe walls	10.5	14.3	7.5
External walls	$t_{air,\infty} = 18\,°C$	$t_{air,\infty} = 18\,°C$	$t_{air,\infty} = 18\,°C$
Tank top wall	4.8	5.5	5.8
Tank side walls	3.8	4.4	5.0
Tank bottom wall	3.4	3.7	4.2

Two values of the heat transfer coefficient for the windings denote their external and internal parts, respectively.

the presented values for the total effective heat transfer coefficients should be considered as only approximate. Values of these temperatures for the particular test case were also gathered in Table 6.

6. Conclusions

The paper describes the experimental validation of a coupled thermal, fluid flow and electromagnetic numerical model of a medium-power dry-type electrical transformer. The coupled computations were carried out to examine the specific power losses within the coils and core. The thermal boundary conditions, i.e. local and temperature-dependent heat fluxes, were determined by considering a numerical model of the surrounding air. Moreover, separate numerical and analytical models were considered in order to obtain the anisotropic thermal conductivities for different types of coils and also for laminated cores. To validate the numerical model, experimental transformer temperature tests in the short-circuit, open-circuit, and under the nominal parameters according to the current European Standards for dry-type transformers were performed. During the tests, temperatures were measured at selected points of the transformer elements using thermocouples, while on external tank walls infrared thermography was employed. As a result, the computed temperatures were compared with the measured values at certain locations and also using infrared photos.

The numerical results showed that the prediction of the temperature distribution within the analyzed transformer and its surroundings was very accurate. Moreover, during the simulations the most effective heat transfer mode for the heat dissipation process was indicated. Furthermore, the procedures developed within this work to handle the coupled thermal, fluid flow and electromagnetic processes in dry-type transformers can also be extended to the most common oil-cooled devices

since this only requires a redefinition of the material properties for the different types of coolant.

It is also worth mentioning that the results obtained from the project can also be used in different types of scientific works. For instance, the effective anisotropic thermal conductivities were developed for different types of coils and these values are usually crucial for the circuit analyses. In addition, the average values of the heat transfer coefficients were calculated based on the local distribution of the wall heat fluxes. This information was obtained for all important transformer elements in terms of the heat transfer. For this reason, the average heat transfer coefficients can be used in simplified analyses, in which the air flow around the transformer is not considered.

Acknowledgements

References

[1] O. Biro, K. Preis, G. Buchgraber, Strong thermal-electromagnetic coupling in FEM simulation of power transformers, in: Proceedings of Int. Conf. on Computational Methods for Coupled Problems in Science and Engineering, Coupled Problems 2005, Santorini, Greece, 2005.

[2] A. Lefevre, L. Miegeville, J. Fouladgar, G. Olivier, 3-D computation of transformer overheating under nonlinear loads, IEEE Trans. Magnetics 30 (2005) 1564–1567.

[3] K. Preis, O. Biro, I. Ticar, FEM analysis of eddy current losses in nonlinear laminated cores, IEEE Trans. Magnetics 41 (2005) 1412–1415.

[4] J.-M. Mufuta, E. van den Bulck, Modelling of mass flow distribution around an array of rectangular blocks in-line arranged and simulating the cross-section of a winding disc-type transformer, Appl. Thermal Engrg. 21 (2001) 731–749.

[5] J.-M. Mufuta, E. van den Bulck, Modelling of the mixed convection in the windings of a disc-type power transformer, Appl. Thermal Engrg. 20 (2000) 417–437.

[6] H.-M. Chang, Y.S. Choi, S.W. van Sciver, K.D. Choi, Cryogenic cooling system of HTS transformers by natural convection liquid nitrogen, Cryogenics 43 (2003) 589–596.

[7] K.U. Joshi, N.K. Deshmukh, Thermal analysis of oil cooled transformer, in: Proceedings of Cigre 2004 Session, Paris, France, 2004.

[8] G. Swift, T.S. Molinski, A fundamental approach to transformer thermal modeling—part I: Theory and equivalent circuit, IEEE Trans. Power Delivery 16 (2001) 171–175.

[9] Z. Radakovic, S. Maksimovic, Non-stationary thermal model of indoor transformer stations, Electrical Engrg. 84 (2002) 109–117.

[10] S.A. Ryder, A simple method for calculating winding temperature gradient in power transformers, IEEE Trans. Power Delivery 17 (2002) 637–642.

[11] D.T. Lussier, R.M. Ormiston, R.M. Marko, Theoretical determination of anisotropic effective thermal conductivity in transformer windings, Int. Comm. Heat Mass Transfer 30 (2003) 313–322.

[12] J. Lehtonen, R. Mikkonen, J. Paasi, Effective thermal conductivity in HTS coils, Cryogenics 40 (2000) 245–249.

[13] J. Smolka, D.B. Ingham, L. Elliott, A.J. Nowak, Enhanced numerical model of performance of an encapsulated three-phase transformer in laboratory environment, Appl. Thermal Engrg. 27 (2007) 156–166.

[14] Dry-type power transformers, European Standard EN 60726:2003.

[15] Fluent Product Documentation, www.fluent.com.

[16] Ansys Product Documentation, www.ansys.com.

[17] Catia Product Documentation, www.3ds.com.

[18] J. Smolka, A.J. Nowak, L.C. Wrobel, Numerical modelling of thermal processes in an electrical transformer dipped into polymerised resin by using commercial CFD package Fluent, Computers & Fluids 33 (2004) 859–868.

[19] J. Smolka, Numerical Analysis of Heat Transfer Processes within Selected Electrical Transformers, Ph.D. thesis, Silesian University of Technology, Poland, 2006.

[20] M.N. Ozisik, Heat Transfer. A Basic Approach, McGraw–Hill, New York, 1985.

[21] J.D. Anderson, Computational Fluid Dynamics. The Basics with Applications, McGraw–Hill, New York, 1995.

[22] J. Blazek, Computational Fluid Dynamics: Principles and Applications, Elsevier, Oxford, 2001.

[23] A.G. Fedorow, R. Viscanta, Turbulent natural convection heat transfer in an asymmetrically heated, vertical parallel-plate channel, Int. J. Heat Mass Transfer 40 (1997) 3849–3860.

[24] L. Shao, S.B. Riffat, Accuracy of CFD for predicting pressure losses in HVAC duct fittings, Appl. Energy 51 (1995) 233–248.

[25] A. Behzadmehr, N. Galanis, A. Laneville, Low Reynolds number mixed convection in vertical tubes with uniform wall heat flux, Int. J. Heat Mass Transfer 46 (2003) 4823–4833.

[26] J.K. Sigey, F.K. Gatheri, M. Kinyanjui, Numerical study of free convection turbulent heat transfer in an enclosure, Energy Conversion and Management 45 (2004) 2571–2582.

[27] B.E. Launder, B.I. Sharma, Application of the energy dissipation model of turbulence to the calculation of flow near a spinning disc, Let. Heat Mass Transfer 1 (1974) 131–138.

[28] E.H. Chui, G.D. Raithby, Computation of radiant heat transfer on a non-orthogonal mesh using the Finite-Volume method, Numer. Heat Transfer, Part B 23 (1993) 269–288.

[29] J.Y. Murthy, S.R. Mathur, A Finite Volume Method for radiative heat transfer using unstructured meshes, Proceedings of American Institute of Aeronautics and Astronautics Conference (AIAA-98-0860), 1998.

[30] J.P. Holman, Heat Transfer, DCW Industries Inc., La Canada, 1998.

[31] N.N. Rao, Elements of Engineering Electromagnetics, Prentice Hall, New Jersey, 1994.

[32] O. Biro, K. Preis, On the use of the magnetic vector potential in the finite element analysis of the three-dimensional eddy currents, IEEE Trans. Magnetics 25 (1989) 3145–3159.

[33] E.C. Snelling, Soft Ferrites. Properties and Applications, Butterwoths Publishing, Stoneham, 1988.

[34] J. Reinert, A. Brockmeyer, R.W. De Doncker, Calculation of losses in ferro- and ferrimagnetic materials based on the modified Steinmetz equation, IEEE Trans. Industry Appl. 37 (2001) 1055–1061.

[35] C. Le Niliot, P. Gallet, Infrared thermography applied to the resolution of inverse heat conduction problems: recovery of heat line sources and boundary conditions, Revue Generale de Thermique 37 (1998) 629–643.

[36] E.R. Meinders, T.H. van der Meer, K. Hanjalic, C.J.M. Lasance, Application of infrared thermography to the evaluation of local convective heat transfer on arrays of cubical protrusions, Int. J. Heat Mass Transfer 18 (1997) 2571–2582.

[37] Guide for the verification and validation of computational fluid dynamics simulations, AIAA-G-077-1998, American Institute of Aeronautics and Astronautics, Reston, VA, 1998.

[38] Power transformers. European Standard EN 60076:1997.

[39] Transformer manufacturer's technical documentation, Areva T&D Mikolow, Poland.